RSC Advances

ROYAL SOCIETY OF CHEMISTRY

www.rsc.org/advances

Journal Name

COMMUNICATION

$MoSe_2$ Nanosheets Grown on Carbon Cloth with Superior Electrochemical Performance as Flexible Electrode for Sodium Ion Batteries

Received 00th January 20xx,
Accepted 00th January 20xx

DOI: 10.1039/x0xx00000x

www.rsc.org/

Yi Zhang†, Zhengqing Liu†, Hongyang Zhao and Yaping Du*

Flexible $MoSe_2$/CF composite has been synthesized by a simple solvothermal method. $MoSe_2$ nanosheets with a thickness of 20 nm are grown uniformly on the surface of the carbon fibers. The $MoSe_2$/CF can be used as self-supporting anode directly with superior electrochemical performance for sodium ion battery.

After the discovery of graphene, two dimensional materials such as black phosphorus,[1-3] MXenes[4-7] and MX_2 (M = V, Mo or W and X = S or Se)[8-23] have been widely investigated in recent years. The MX_2 is layered transition-metal dichalcogenides (TMD) that hexagonal layers of M are sandwiched between two X layers. The X-M-X interactions are covalently bonded while the nearby X layers are connected by weak van der Waals interaction, which allow a variety of ions to intercalate between the X-X layers.[24, 25] Due to these features, MX_2 has shown intriguing physical and chemical properties as well as versatile advanced applications such as solid lubrication,[26] solar cell[27-29] and hydrogen evolution catalysts.[29-32] Among the MX_2, molybdenum disulfide (MoS_2) has been investigated intensively as energy storage materials since Li-ions and Na-ions can insert reversibly in the S-S layered space.[8-11, 33, 34] For example, the electrochemical reactions in a Na-MoS_2 battery is based on intercalation and conversion: During the electrochemical process, the Na^+ ions first intercalate into the S-S layered space of MoS_2 to form $NaxMoS_2$ and then the $NaxMoS_2$ converts into Mo and Na_2S.[11] Though the theoretical capacity of MoS_2 is very high when acted as anode material for sodium ion battery, there are several inherent defects impede its further application; the inherent low electric conductivity and the small layer distance lead to inferior rate ability and rapid capacity decay.[19]

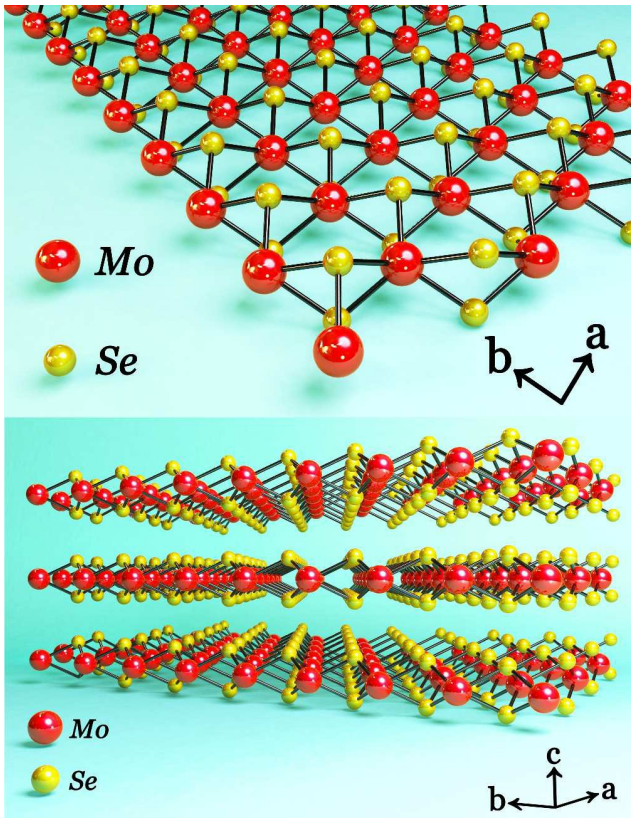

Fig. 1 Crystal structure of the hexagonal MoSe2 (Se-Mo-Se layer and Se-Se layer space).

$MoSe_2$, as a close analogue to MoS_2, can also be viewed as three stacked atom layers (Se-Mo-Se) held together by the van der Waals force (Fig. 1). What's more, the $MoSe_2$ has smaller band gap and larger layer space than that of MoS_2,[35] indicating its better electric conductivity and coulombic efficiency when acted as anode material for sodium ion battery.[19] However, the electrochemical performance of $MoSe_2$ for sodium ion battery has been rarely investigated so far.[19-21]

Frontier Institute of Science and Technology jointly with College of Science, State Key Laboratory for Mechanical Behavior of Materials, Xi'an Jiaotong University, 99 Yanxiang Road, Yanta District, Xi'an Shaanxi Province 710054, China, E-mail: ypdu2013@mail.xjtu.edu.cn.
† These authors contributed equally to this work.
Electronic Supplementary Information (ESI) available: Full experimental procedures, experimental Section, EDAX spectra, TEM images, XRD pattern and other electrochemical performance data. See DOI: 10.1039/x0xx00000x

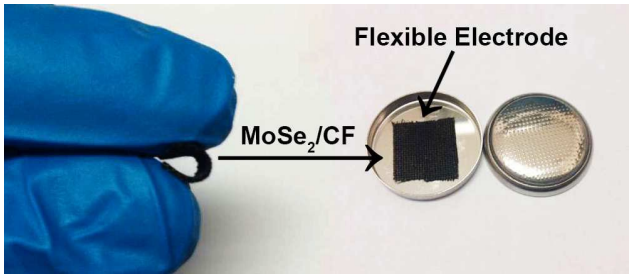

Fig. 2 Optical image of the synthesized $MoSe_2$/CF sample.

Flexible electrode design is quite attractive for next-generation energy storage with superior rate ability and high energy density since this kind of electrode has lighter weight and higher electric conductivity than conventional electrode (the conventional electrode includes active materials, carbon additive, binder and metal current collector).[36] Carbon cloth is a kind of porous 3D flexible substrate consisting of carbon fibres with highly textured surface. Towards the achievement of flexible electrode with high electrochemical performance for SIB, in this communication, we design $MoSe_2$/carbon fibre ($MoSe_2$/CF) flexible anode by employing carbon cloth as substrate for the application of sodium ion battery. The $MoSe_2$/CF can be used as electrode directly without binder and carbon additive (Fig. 2). When acted as anode material for sodium ion battery, the $MoSe_2$/CF delivers a high capacity of 452.6 mAh g^{-1} at 0.2 A g^{-1} and can keep 85.5% capacity retention after 100 cycles. Even at a high current density of 5 A g^{-1}, it can still give a high capacity of 161.9 mAh g^{-1}, indicating its strong potential for advanced sodium energy storage.

The $MoSe_2$/CF flexible electrode can be fabricated by a solvothermal reaction. Carbon cloth is employed as flexible substrate for the $MoSe_2$ nanosheets growth. Specifically, 0.5 mmol $(NH_4)_2MoO_4$ and 1 mmol Se powder are added in 18 mL mixture of 9 mL oleic acid and 9 mL ethanol in 20 mL Teflon-lined autoclave. The autoclave is sealed and heated at 180 °C for 72 h in an oven, and then cool down to room temperature. Then the as-prepared $MoSe_2$/CF sample is further annealed in Ar/H_2 (95%/5%) at 300 °C for 1 h to remove the organic residue and excess selenium powder. For comparison, pure $MoSe_2$ nanosheets are also prepared under the same condition without carbon cloth. Detailed preparation procedures are described in Experiment Section and Table 1.

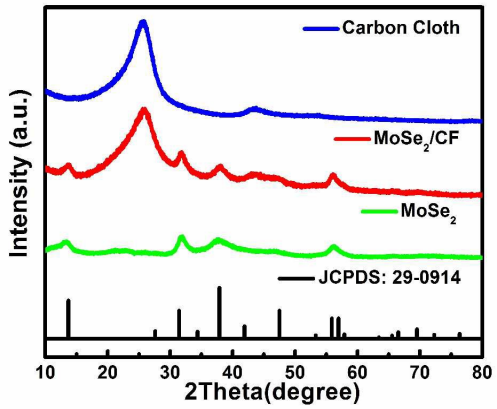

Fig. 3 XRD patterns of the pure $MoSe_2$, $MoSe_2$/CF and carbon cloth samples.

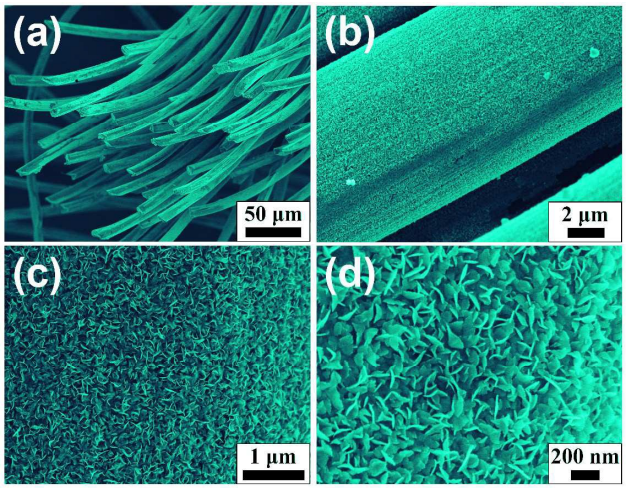

Fig. 4 (a, b, c, d) The SEM images with different magnifications of the $MoSe_2$/CF sample.

The XRD patterns of the annealed products are shown in Fig. 3. The peaks at 26.4°, 44.2° and 55.8° are assigned to the carbon cloth substrate.[37] Other diffraction peaks can be readily indexed to the hexagonal crystal phase with P63/mmc space group of $MoSe_2$ (JCPDS: 29-0914), and no diffraction peaks from any other chemical such as MoO_3 or Se are detectable in both the $MoSe_2$/CF and pure $MoSe_2$ samples.[16] In order to further investigate the chemical nature and bonding state of $MoSe_2$ on the CF surface, the X-ray photoelectron spectroscopy (XPS) spectrum is carried out and the results are shown in Fig. S1. As seen from Fig. S1a, double peaks located at 232.1 and 228.8 eV are ascribed to the core levels of Mo $3d_{3/2}$ and Mo $3d_{5/2}$ of $MoSe_2$, respectively, indicating that the element chemical state of Mo ions are mainly quadrivalent for the $MoSe_2$/CF. Two intense peaks at 54.9 and 54.2 eV (Fig. S1b) attribute to the core levels of Se $3d_{3/2}$ and Se $3d_{5/2}$, respectively, suggesting the characteristic of Se^{2-} in $MoSe_2$/CF.

Fig. 4 shows the typical scanning electron microscopy (SEM) images of the $MoSe_2$/CF sample with different magnifications. As shown in Fig. 4a & b, the surface of the CFs are covered uniformly by densely packed $MoSe_2$ nanosheets. From Fig. 4c & d, we can see that most of the nanosheets are vertically aligned on the CFs. The thickness of the $MoSe_2$ nanosheet is about 20 nm. The SEM images of pure $MoSe_2$ are shown in Fig. S2a. The flower-like nanostructured $MoSe_2$ with average size of 150 nm are formed by $MoSe_2$ nanosheets assembly.

The crystal structure of $MoSe_2$ is examined with high-resolution TEM (HRTEM). Fig. 5a obviously demonstrates the TEM image of $MoSe_2$ nanosheets obtained by sonication of $MoSe_2$/CF sample. Fig. 5b shows HRTEM image taken from the rim of $MoSe_2$ nanosheets in Fig. 5a, the clear-cut crystal lattice fringes with interplanar spacing of ~0.32 nm correspond to the (004) plane of hexagonal (2H-type) $MoSe_2$. The HRTEM image and selected area electron diffraction (SAED) patterns (inset of Fig.5f) suggest that $MoSe_2$ nanosheets have well-defined crystal structure. The TEM images of pure $MoSe_2$ are shown in Fig. S2b.

To investigate the electrochemical behaviour of the $MoSe_2$/CF sample in sodium ion battery, electrochemical characterization have been conducted based on coin cells (metallic sodium serves as

the counter electrode). The loading mass of $MoSe_2$ on $MoSe_2$/CF sample is 0.0026 g. The electrochemical performance of CF are shown in Fig. S3 and the CF provide almost no capacity during the electrochemical process. Fig. 6a shows the cyclic voltammograms (CV) curves for the initial four cycles of $MoSe_2$/CF electrode at a scan rate of 0.2 mV s^{-1} in a voltage range from 0 to 3.0 V vs. Na/Na^+. In the first cathodic sweep, three cathodic peaks at 1.8 V, 1.3 V and 0.35 V can be observed. The peaks at 1.8 V and 1.3 V are correspond to the sodium insertion to $MoSe_2$ to form Na_xMoSe_2 while the following peak at 0.35 V is caused by the formation of Na_2Se and the irreversible decomposition of the electrolyte.[19, 20] During the anodic scan, two oxidation peaks at 0.3 V and 1.8 V can be observed due to the partial oxidation of Mo and Na_2Se.[19, 20] Starting from the second cycle, the electrode displays single peak at 1.3 V while the peaks at 0.35 V and 1.8 V in the first cathodic sweep disappear. In the subsequent process, no obvious changes are observed for the redox peaks, implying the good stability of the electrochemical process. The CV behaviour of pure $MoSe_2$ electrode can be seen in Fig. S4a.

Fig. 6b shows the galvanostatic charge/discharge profiles of the $MoSe_2$/CF in the first, second, 3rd, 10th, 20th, 50th and 100th at a current density of 0.2 A g^{-1}. The anode gives an initial capacity of 887.9 mAh g^{-1} based on the mass of the $MoSe_2$ on the carbon cloth. This large discharge capacity is attributed to the electrolyte decomposition and subsequent formation of the solid electrolyte interface (SEI) layer, which consistent with the above CV analysis. After the initial capacity loss, a capacity of 390.7 mAh g^{-1} is achieved after 100 cycles, and the pattern of discharge and charge profile almost remain unchanged. For comparison, pure $MoSe_2$ are tested under the same condition (Fig. S4b). The first discharge capacity for pure $MoSe_2$ anode was 1088.9 mAh g^{-1}. However, serious capacity decay is observed and the capacity of the pure $MoSe_2$ anode decreases to 282.8 mAh g^{-1} after 100 cycles.

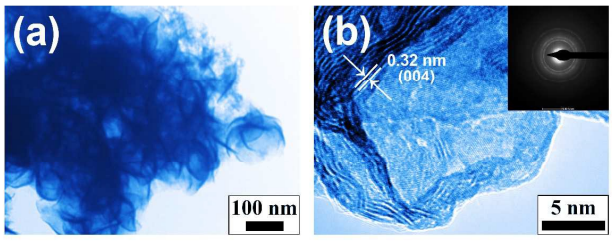

Fig. 5 (a) TEM image of the $MoSe_2$/CF sample. (b) HRTEM image and SAED pattern (inset) of $MoSe_2$/CF sample.

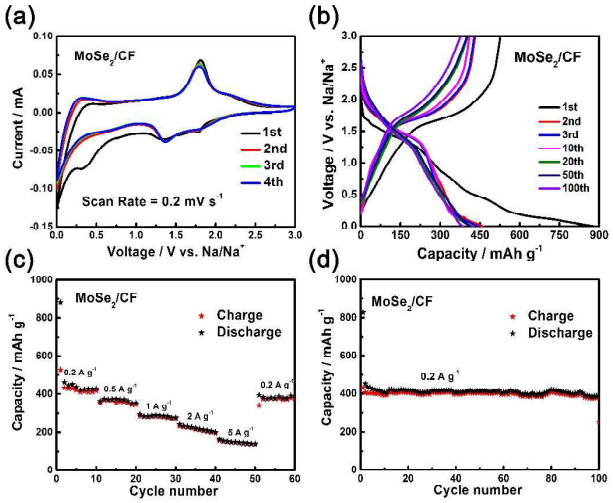

Fig. 6 Electrochemical performance of $MoSe_2$/CF. (a) CV curves at a scan rates of 0.2 mV s^{-1}, b) Charge/discharge curves cycling at 0.2 A g^{-1}, c) Rate performance, d) Cyclic properties at 0.2 A g^{-1}.

Rate performance is an important criterion to evaluate the performance of the material under high current density. Both of the $MoSe_2$/CF and pure $MoSe_2$ are selected for the test of rate capability. Specifically, these two electrodes are cycled from 0.2 to 5 A g^{-1} in steps and then return to 0.2 A g^{-1}. As shown in Fig. 6c, the $MoSe_2$/CF electrode exhibits final discharge capacities of 462.1, 362.2, 294.2, 239.7 and 161.9 mAh g^{-1} at current densities of 0.2, 0.5, 1, 2 and 5 A g^{-1}, respectively. It should be noted that such rate capability could be used in the design of sodium storage for high power-oriented application. After 50 cycles of charge and discharge at a various current densities, the discharge capacity of the $MoSe_2$/CF hybrid nanostructures electrode can still recover to 394.3 mAh g^{-1} at 0.2 A g^{-1}, indicating the outstanding rate performance and resilience of the electrode. In contrast, pure $MoSe_2$ electrode exhibits poor rate capability (Fig. S4c). It gives only 115.4 mAh g^{-1} at 5 A g^{-1} and can not recover its initial level when the current density returns to 0.2 A g^{-1}. For better comparison, the rate ability of $MoSe_2$/CF and $MoSe_2$ are merged in one picture as shown in Fig. S5a. This difference suggests that the carbon cloth can serve as conductive pathway to facilitate the electronic/ionic migration.

Cycling performance of the $MoSe_2$/CF and pure $MoSe_2$ are evaluated by galvanostatic measurement at current density of 0.2 A g^{-1}. As shown in Fig. 6d, the first cycle lost of $MoSe_2$/CF bybrid nanostructures electrode can be attributed to the SEI formation on the composite surface. After the first cycle, $MoSe_2$/CF electrode delivers a noticeable capacity of 452.6 mAh g^{-1} and there is 85.5% retention throughout 100 cycles at 0.2 A g^{-1}. In contrast, large capacity decay can be observed for pure $MoSe_2$ electrode after 100 cycles at 0.2 A g^{-1} (Fig. S4d). For better comparison, the cycling stability of $MoSe_2$/CF and $MoSe_2$ are merged in one picture as shown in Fig. S5b. The superior cycling stability and rate ability of $MoSe_2$/CF electrode can certainly be credited to the presence of carbon cloth since it offers a substrate for $MoSe_2$ nanosheets uniformly growing on the surface of the CF, which in turn enlarge the interface reaction area between the electrode and electrolyte. What's more, the porous structure of 3D flexible carbon cloth can

facilitate the penetration of electrolyte and provide conductive pathway for electron transfer (Fig. 7). The SEM images of $MoSe_2$/CF samples after 100 cycles at 0.2 A g^{-1} are shown in Fig. S6.

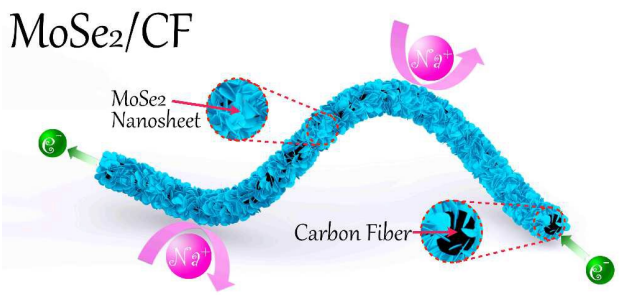

Fig. 7 Pathways for electron conduction and sodium ion diffusion during electrochemical reaction process of the $MoSe_2$/CF flexible electrode.

Conclusions

In summary, flexible $MoSe_2$/CF composite has been synthesized by an efficient solvothermal method. The $MoSe_2$/CF sample can be employed as electrode material directly without binder and carbon additive. The $MoSe_2$ nanosheets are grown uniformly on CF so that the interface reaction area between electrode and electrolyte can be enlarged and the CF can act as conductive pathway for fast electron-transfer. When tested as anode material for sodium ion battery, it can deliver a stable discharge capacity of 452.6 mAh g^{-1} and keep 85.5% retention after 100 cycles at 0.2 A g^{-1}, even at a high current density of 5 A g^{-1}, a high discharge capacity of 161.9 mAh g^{-1} is still achieved. The superior rate ability and cycling stability of the $MoSe_2$/CF flexible electrode suggests its outstanding performance as anode material for advanced sodium energy storage.

Acknowledgements

We gratefully acknowledge the financial aid from the start-up funding from Xi'an Jiaotong University, the Fundamental Research Funds for the Central Universities (2015qngz12), the NSFC (grant no. 21371140), and the China National Funds for Excellent Young Scientists (grant no. 21522106). We also appreciated Dr. Xing-Hua Li in Northwest University for his kind helps to obtain HRTEM images. We also highly appreciated Prof. Yunhui Huang from Huazhong University of Science and Technology, China, for his kind helps and valuable discussions.

Notes and references

1. R. Fei and L. Yang, *Nano Letters*, 2014, **14**, 2884-2889.
2. D. Wang, N. Chen, M. Li, C. Wang, H. Ehrenberg, X. Bie, Y. Wei, G. Chen and F. Du, *J. Mater. Chem. A*, 2015, **3**, 8636-8642.
3. Z. Jian, W. Han, Y. Liang, Y. Lan, Z. Fang, Y.-S. Hu and Y. Yao, *J. Mater. Chem. A*, 2014, **2**, 20231-20236.
4. M. Naguib, V. N. Mochalin, M. W. Barsoum and Y. Gogotsi, *Adv. Mater.*, 2014, **26**, 992-1005.
5. M.-S. Song, R.-H. Kim, S.-W. Baek, K.-S. Lee, K. Park and A. Benayad, *J. Mater. Chem. A*, 2014, **2**, 631-636.
6. S. S. Zhang, K. Xu and T. R. Jow, *J. Electrochem. Soc.*, 2002, **149**, A1521-A1526.
7. X. Wang, S. Kajiyama, H. Iinuma, E. Hosono, S. Oro, I. Moriguchi, M. Okubo and A. Yamada, *Nat Commun*, 2015, **6**.
8. L. David, R. Bhandavat and G. Singh, *ACS Nano*, 2014, **8**, 1759-1770.
9. D. W. Su, S. X. Dou and G. X. Wang, *Adv. Energy Mater.*, 2015, **5**, DOI: 10.1002/Aenm.201401205..
10. X. Xie, Z. Ao, D. Su, J. Zhang and G. Wang, *Adv. Funct. Mater.*, 2015, **25**, 1393-1403.
11. Z. Hu, L. Wang, K. Zhang, J. Wang, F. Cheng, Z. Tao and J. Chen, *Angew. Chem. Int. Ed.*, 2014, **53**, 12794-12798.
12. B. Liu, T. Luo, G. Mu, X. Wang, D. Chen and G. Shen, *ACS Nano*, 2013, **7**, 8051-8058.
13. D. Su, S. Dou and G. Wang, *Chem Commun (Camb)*, 2014, **50**, 4192-4195.
14. Y. Liu, N. Zhang, H. Kang, M. Shang, L. Jiao and J. Chen, *Chemistry – A European Journal*, 2015, **21**, 11878-11884.
15. S. H. Choi and Y. C. Kang, *Nanoscale*, 2015, **7**, 3965-3970.
16. Y. Shi, C. Hua, B. Li, X. Fang, C. Yao, Y. Zhang, Y.-S. Hu, Z. Wang, L. Chen, D. Zhao and G. D. Stucky, *Adv. Funct. Mater.*, 2013, **23**, 1832-1838.
17. Y. Liu, M. Zhu and D. Chen, *J. Mater. Chem. A*, 2015, **3**, 11857-11862.
18. H. Wang, X. Wang, L. Wang, J. Wang, D. Jiang, G. Li, Y. Zhang, H. Zhong and Y. Jiang, *J. Phys. Chem. C*, 2015, **119**, 10197-10205.
19. H. Wang, X. Lan, D. Jiang, Y. Zhang, H. Zhong, Z. Zhang and Y. Jiang, *J. Power Sources*, 2015, **283**, 187-194.
20. Y. N. Ko, S. H. Choi, S. B. Park and Y. C. Kang, *Nanoscale*, 2014, **6**, 10511-10515.
21. X. Yang, Z. Zhang, Y. Fu and Q. Li, *Nanoscale*, 2015, **7**, 10198-10203.
22. J. Feng, X. Sun, C. Wu, L. Peng, C. Lin, S. Hu, J. Yang and Y. Xie, *J. Am. Chem. Soc.*, 2011, **133**, 17832-17838.
23. J.-Y. Liao and A. Manthiram, *Nano Energy*, 2015, **18**, 20-27.
24. J. Hassoun, F. Croce, I. Hong and B. Scrosati, *Electrochem. Commun.*, 2011, **13**, 228-231.
25. S. Brutti, J. Hassoun, B. Scrosati, C.-Y. Lin, H. Wu and H.-W. Hsieh, *J. Power Sources*, 2012, **217**, 72-76.
26. R. Verrelli, J. Hassoun, A. Farkas, T. Jacob and B. Scrosati, *J. Mater. Chem. A*, 2013, **1**, 15329-15333.
27. E. Gourmelon, O. Lignier, H. Hadouda, G. Couturier, J. C. Bernède, J. Tedd, J. Pouzet and J. Salardenne, *Solar Energy Materials and Solar Cells*, 1997, **46**, 115-121.
28. G. A. Elia, S. Panero, A. Savoini, B. Scrosati and J. Hassoun, *Electrochim. Acta*, 2013, **90**, 690-694.
29. A. Moretti, M. Secchiaroli, D. Buchholz, G. Giuli, R. Marassi and S. Passerini, *J. Electrochem. Soc.*, 2015, **162**, A2723-A2728.
30. Y. Xu, E. Memarzadeh Lotfabad, H. Wang, B. Farbod, Z. Xu, A. Kohandehghan and D. Mitlin, *Chem. Commun.*, 2013, **49**, 8973-8975.
31. S.-M. Oh, S.-T. Myung, C. S. Yoon, J. Lu, J. Hassoun, B. Scrosati, K. Amine and Y.-K. Sun, *Nano Letters*, 2014, **14**, 1620-1626.
32. H. Ming, J. Ming, S.-M. Oh, S. Tian, Q. Zhou, H. Huang, Y.-K. Sun and J. Zheng, *ACS Appl. Mater. Interfaces*, 2014, **6**, 15499-15509.
33. C. Zhu, X. Mu, P. A. van Aken, Y. Yu and J. Maier, *Angew. Chem. Int. Ed.*, 2014, **53**, 2152-2156.
34. K. Chang and W. Chen, *ACS Nano*, 2011, **5**, 4720-4728.
35. S. Balendhran, S. Walia, H. Nili, J. Z. Ou, S. Zhuiykov, R. B. Kaner, S. Sriram, M. Bhaskaran and K. Kalantar-zadeh, *Adv. Funct. Mater.*, 2013, **23**, 3952-3970.
36. G. Zhou, F. Li and H.-M. Cheng, *Energy. Environ. Sci.*, 2014, **7**, 1307-1338.

37. S. Y. Lim, H. Kim, R. A. Shakoor, Y. Jung and J. W. Choi, *J. Electrochem. Soc.*, 2012, **159**, A1393-A1397.